Finite Element Formulations for Systems with High-Temperature Superconductors

Julien Dular, Christophe Geuzaine, and Benoît Vanderheyden

Abstract—**In this paper, we consider finite element models for high-temperature superconductors and compare two dual formulations, either magnetic-field conforming or magnetic-flux-density conforming. The electrical resistivity of superconductors is described by a power law and is strongly nonlinear. We compare the accuracy and the efficiency of the dual formulations by starting from simple considerations on the concavity / convexity of the constitutive law involved in each case. We then study the numerical behavior of each formulation in 1D, 2D, and 3D problems and compare their results against benchmarks. We draw general recommendations for the choice of a formulation, an iteration scheme for treating the corresponding linearized constitutive law, and a time-stepping extrapolation scheme. This approach is extended to soft ferromagnetic materials with a saturation law. Since the outcome of our analysis shows that recommended formulations for treating ferromagnets are just the opposite of those for treating superconductors, we suggest a coupled formulation for systems where both types of materials are present. The coupled formulation is shown to be accurate and more efficient than single formulations applied indistinctly to all materials.**

Index Terms—**Finite element analysis, high-temperature superconductors, magnetic materials, nonlinear equations.**

I. Introduction

MODELING accurately and efficiently the magnetic response of high-temperature superconductors (HTS) is of high importance in numerous applications, such as energy transport and storage [1], trapped-field magnets, magnetic shields, and levitating devices [2]. Among the existing numerical methods, the finite element (FE) method allows one to tackle complex geometries and is commonly used for the design and analysis of engineering devices [3]. The FE method expresses the problem in a weak form and different formulations of the same problem are available. More specifically in the framework of magnetodynamics, two classes of dual formulations exist: h-conform formulations, that respect the continuity conditions for magnetic fields, and b-conform ones, that guarantee the continuity of magnetic flux. These two classes involve the HTS nonlinear laws in inverse ways, through either the electrical resistivity or the electrical conductivity, and thus may exhibit different numerical behaviors. Earlier investigations of h-conform formulations for solving superconductor systems can be found in [4], [5] for the h-formulation, and in [6], [7], [8], [9] for t-ω formulations. Similar works on b-conform formulations can be found in [6], [8], [10], [11], [12], [13] for a-v formulations. To date, a few

comparisons of the different formulations have been conducted in the literature, see for instance [6] for a comparison of a-v and t-ω formulations in 2D with a Newton-Raphson time stepping scheme, [14] for a comparison of the h-, t-ω- and a-v-j-formulations in 2D, [3] for an overview and [15] for a summary of methods for computing AC losses. In parallel, several benchmark problems have been developed over the years to serve as reference problems [16]. However, as pointed out in [3], there are still few comparisons based on simulations which are carried out within the same environment and are validated against benchmarks, so that it is difficult to draw general conclusions on the performance of the different approaches.

The purpose of this work is to implement and study two FE formulations, a magnetic-field conforming formulation (here an h-ϕ-formulation) and a magnetic-flux-density conforming formulation (here an a-formulation), and compare their performance using the same numerical environment. No a priori is made on their behavior and several time-stepping schemes, as well as different iterative techniques, are systematically investigated.

The manuscript is organized as follows: the different FE models and formulations are presented in Sec. II. In Sec. III, we start from simple considerations on the treatment of the nonlinear constitutive law by iterative techniques (Picard and Newton-Raphson). We then discuss the advantages and drawbacks of each formulation based on their accuracy and efficiency in 1D, 2D, and 3D problems, together with a validation against known solutions and benchmarks. In Sec. IV, we adopt a similar approach for soft ferromagnetic materials with a magnetic saturation law. As it turns out that the a-formulation is the best performing one for ferromagnets, whereas the h-ϕ-formulation is preferred for superconductors, we suggest a coupled formulation for situations where both types of materials are present. We show that such an approach yields accurate results with a better efficiency than single formulations. Our final conclusions are drawn in Sec. V.

Model files for the main test cases are available on the website www.life-hts.uliege.be.

II. Model and FE Formulations

A. Physical model

We consider the magnetic response of a system containing type-II superconductors with strong pinning that are cooled in a cryogenic fluid or placed in the cold chamber of a measurement device.

Maxwell's equations are solved in the magnetodynamic approximation [17], where the displacement current is neglected,

$$\begin{cases} \operatorname{div} \boldsymbol{b} = 0, \\ \operatorname{\boldsymbol{curl}} \boldsymbol{h} = \boldsymbol{j}, \\ \operatorname{\boldsymbol{curl}} \boldsymbol{e} = -\partial_t \boldsymbol{b}, \end{cases} \tag{1}$$

with $\boldsymbol{b}$, $\boldsymbol{h}$, $\boldsymbol{j}$, $\boldsymbol{e}$ the magnetic flux density (T), the magnetic field (A/m), the electric current density (A/m^2), and the electric field (V/m), respectively. The system is composed of non-conducting materials (but possibly magnetic ones), for which $\boldsymbol{b} = \mu(\boldsymbol{h})\boldsymbol{h}$ and $\boldsymbol{j} = \boldsymbol{0}$, together with superconductors, described by $\boldsymbol{b} = \mu_0\boldsymbol{h}$ (assuming $\|\boldsymbol{h}\| \gg H_{c1}$) and the $\boldsymbol{e}$-$\boldsymbol{j}$ power law [18],

$$\boldsymbol{j} = \frac{j_c}{e_c}\left(\frac{\|\boldsymbol{e}\|}{e_c}\right)^{(1-n)/n} \boldsymbol{e}, \tag{2}$$

where e_c (V/m) is a threshold electric field defining the critical current density j_c (A/m^2). By convention, e_c is often chosen to be 10^{-4} V/m. The dimensionless exponent $n = U_0/k_B T$ describes the sharpness of the transition to flux flow, where U_0 is the pinning energy barrier and $k_B T$ the thermal energy ($k_B = 1.38 \times 10^{-23}$ J/K is the Boltzmann constant).

B. Finite Element Formulations

The system is represented by a domain Ω that is decomposed into a conducting domain, Ω_c, defined as an open set and containing the superconducting materials, and its complementary domain, Ω_c^C, a closed set containing the other, electrically insulating, materials. Boundary conditions are applied on the external boundary, $\partial\Omega$, which is decomposed into two complementary domains: Γ_e, where the normal component of $\boldsymbol{b}$ or the tangential component of $\boldsymbol{e}$ is imposed, and Γ_h, where the tangential component of $\boldsymbol{h}$ is imposed.

The non-conducting domain Ω_c^C can be simply or multiply connected. Multiply connected geometries typically occur in the presence of an external source. They can be made simply connected by introducing cuts [19], as illustrated in Fig. 1 for the case of a tape with an imposed current.
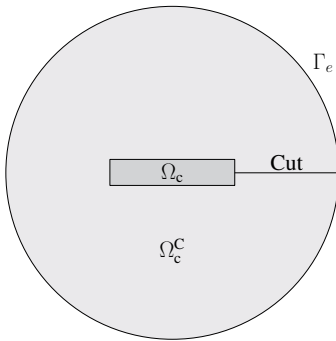

Fig. 1: Example of a problem domain (*tape case of section III-B, scale not respected*) with a current imposed across Ω_c. The problem is 2D and contains a single conducting region. The cut makes Ω_c^C simply connected. The external boundary belongs to Γ_e as $\boldsymbol{b} \cdot \boldsymbol{n}|_{\Gamma_e} = 0$ can be assumed provided Γ_e is far enough from the conductor.

An injected current intensity I and an applied voltage V are associated to each connected region of Ω_c and are thus defined as global quantities. Exactly one of these quantities is fixed in each region (coupling with circuit equations is not considered here). If the domain Ω_c is made up of N connected parts $\Omega_{c,i}$ with $i \in C = \{1, 2, \ldots, N\}$, the current intensity is imposed in a subset C_I of C and the voltage is imposed in the complementary set C_V.

A finite element mesh is generated to discretize the domain. Nodes, edges and facets of the conducting domain boundary belong to the closed set Ω_c^C.

Magnetic field conform formulation (h-formulation): The chosen h-conform formulation expresses the magnetodynamic problem in terms of $\boldsymbol{h}$ discretized with Whitney elements [20] as follows:

$$\boldsymbol{h} = \sum_{e \in \Omega_c} h_e \,\boldsymbol{\psi}_e + \sum_{n \in \Omega_c^C} \phi_n \,\mathbf{grad}\,\psi_n + \sum_{i \in C} I_i \,\boldsymbol{c}_i, \tag{3}$$

with $\boldsymbol{\psi}_e$ the edge function of edge e, ψ_n the node function of node n, and $\boldsymbol{c}_i$ a discontinuous shape function associated with the cut related to conducting region i, defined on a transition layer [21]. Coefficients h_e, ϕ_n and I_i are the degrees of freedom of the problem. The decomposition in (3) confers two properties to $\boldsymbol{h}$. First, using gradients in Ω_c^C ensures that $\boldsymbol{h}$ is curl-free in the non-conducting domain. No spurious current density is introduced, and there is no need to consider a large electrical resistivity in these regions. Second, the shape functions $\boldsymbol{c}_i$ directly implement the current constraints in the function space, rather than through an additional integration constraint.

Essential conditions, $\boldsymbol{h}\times\boldsymbol{n}|_{\Gamma_h}$ and I_i for $i \in C_I$, are strongly imposed by fixing the corresponding degrees of freedom: h_e for $e \in \Gamma_h$, ϕ_n for $n \in \Gamma_h$, and I_i for $i \in C_I$. The resulting space for $\boldsymbol{h}$, after imposing essential conditions, is denoted by $\bar{S}_h^1$.

Test functions $\boldsymbol{h}'$ are chosen in the same space (Galerkin scheme), with coefficients h'_e, ϕ'_n and I'_i, but however with vanishing coefficients where essential conditions are imposed. The space of test functions is denoted as $\bar{S}_{h0}^1$.

The resulting weak formulation reads [21], [22]:

From an initial solution at time $t = 0$, find $\boldsymbol{h} \in \bar{S}_h^1$ such that, for $t > 0$,

$$\begin{aligned} &\left(\partial_t(\mu(\boldsymbol{h})\,\boldsymbol{h})\,,\boldsymbol{h}'\right)_\Omega + \left(\rho(\mathbf{curl}\,\boldsymbol{h})\,\mathbf{curl}\,\boldsymbol{h}\,,\mathbf{curl}\,\boldsymbol{h}'\right)_{\Omega_c} \quad (4) \\ &- \left\langle \boldsymbol{e}\times\boldsymbol{n}\,,\boldsymbol{h}'\right\rangle_{\Gamma_e} + \sum_{i \in C} V_i \mathcal{I}_i(\boldsymbol{h}') = 0, \; \forall \boldsymbol{h}' \in \bar{S}_{h0}^1, \end{aligned}$$

where the following notations are used for volume and surface integrals:

$$\left(\bar{A}\,,\bar{B}\right)_\Omega = \int_\Omega \bar{A}\cdot\bar{B}\,d\Omega, \; \left\langle\bar{A}\,,\bar{B}\right\rangle_\Gamma = \int_\Gamma \bar{A}\cdot\bar{B}\,d\Gamma, \tag{5}$$

with $\bar{A}$ and $\bar{B}$ two scalar or vector fields and $\cdot$ the scalar multiplication or the dot product, respectively, and with $\mathcal{I}_i(\boldsymbol{h}) = I_i$. For example, when $\boldsymbol{h}' = \boldsymbol{c}_i$ is chosen ($i \in C_V$, $I'_i = 1$), one obtains the circuit equation

$$\left(\partial_t(\mu\,\boldsymbol{h})\,,\boldsymbol{c}_i\right)_\Omega + \left(\rho\,\mathbf{curl}\,\boldsymbol{h}\,,\mathbf{curl}\,\boldsymbol{c}_i\right)_{\Omega_c} = -V_i. \tag{6}$$

The formulation (4) is referred to as the h-ϕ-formulation or, equivalently, the h-formulation. It is a weak form of Faraday's

equation. The continuity of the tangential component of $\boldsymbol{h}$ is enforced by the considered shape functions. The natural constraints, involving the tangential component of the electric field, $\boldsymbol{e} \times \boldsymbol{n}|_{\Gamma_e}$ and the potentials V_i for $i \in C_V$, are weakly imposed.

In practice, the h-formulation can be solved in one of two ways. Either the total magnetic field $\boldsymbol{h}$ is considered as the unknown, leading to the total h-formulation, or $\boldsymbol{h}$ is decomposed into a known source field $\boldsymbol{h}_{\mathrm{s}}$ and an unknown reaction field $\boldsymbol{h}_{\mathrm{r}}$, $\boldsymbol{h} = \boldsymbol{h}_{\mathrm{s}} + \boldsymbol{h}_{\mathrm{r}}$, leading to the reaction h-formulation.

Note that other h-conform formulations exist, such as the t-ω-formulation. Because the nonlinear constitutive law is involved in the same manner (resistivity), the main numerical behavior is expected to be similar.

Magnetic flux density conform formulation (a-formulation): Gauss's law, div $\boldsymbol{b} = 0$, implies that the magnetic flux density can be expressed in terms of a vector potential $\boldsymbol{a}$ such that $\boldsymbol{b} = \mathbf{curl}\ \boldsymbol{a}$. Faraday's law can then be rewritten as $\mathbf{curl}\ (\boldsymbol{e} + \partial_t \boldsymbol{a}) = \boldsymbol{0}$ so that $\boldsymbol{e} = -\partial_t \boldsymbol{a} - \mathbf{grad}\ v$, with v an electric scalar potential. A gauge condition is necessary to guarantee the uniqueness of the vector potential.

We first consider 3D geometries and 2D geometries with an in-plane current density (for instance, a long bar in a parallel magnetic field). The potentials $\boldsymbol{a}$ and v are discretized with Whitney elements as follows:

$$\boldsymbol{a} = \sum_{e \in \Omega} a_e\ \boldsymbol{\psi}_e \quad \text{and} \quad v = \sum_{i \in C} V_i v_i, \tag{7}$$

with $\boldsymbol{\psi}_e$ the edge function of edge e and v_i a discontinuous shape function associated with a cross-section of conducting region i, known as the generalized source potential [23]. Coefficients a_e and V_i are the degrees of freedom. The shape functions v_i allow one to introduce voltage constraints directly in the basis function, rather than through an integral constraint. Here, the function v_i has a support limited to a transition layer, so that v is not the usual electrostatic potential, see [23].

Essential conditions, $\boldsymbol{e} \times \boldsymbol{n}|_{\Gamma_e}$ and V_i for $i \in C_V$, are strongly imposed by fixing the corresponding degrees of freedom, a_e for $e \in \Gamma_e$ and V_i for $i \in C_V$. The resulting space for $\boldsymbol{a}$, after imposing essential conditions, is denoted by S_e^1. The space for v, after imposing essential conditions, is denoted by S_e^0. The potential $\boldsymbol{a}$ is unique in Ω_{c}, it is a primitive for $\boldsymbol{e}$, $\boldsymbol{e} = -\partial_t \boldsymbol{a}$, but it is not unique in Ω_{c}^C, where $\boldsymbol{e}$ is not evaluated. A gauge must then be introduced in Ω_{c}^C and the resulting space is renamed as $\tilde{S}_e^1$. One convenient gauge, named the co-tree gauge, consists in (strongly) imposing vanishing coefficients on edges that belong to an appropriate tree [24]. Another possibility is to (weakly) impose a Coulomb gauge [24].

Test functions $\boldsymbol{a}'$ and v' are chosen in the spaces defined in (7), with coefficients a_e' and V_i', respectively, but however with vanishing coefficients where essential conditions are imposed. The spaces of test functions are denoted as $\tilde{S}_{e0}^1$ and S_{e0}^0, respectively.

Given the nonlinear conductivity $\sigma = \sigma(-\partial_t \boldsymbol{a} - \mathbf{grad}\ v)$ and reluctivity $\nu = \nu(\mathbf{curl}\ \boldsymbol{a})$, the weak formulation reads as

follows [23], [25]:

From an initial solution at time $t = 0$, find $\boldsymbol{a} \in \tilde{S}_e^1$ and $v \in S_e^0$ such that, for $t > 0$,

$$\begin{aligned} (\nu\ \mathbf{curl}\ \boldsymbol{a}\ ,\mathbf{curl}\ \boldsymbol{a}')_{\Omega} &- \langle \boldsymbol{h} \times \boldsymbol{n}\ ,\boldsymbol{a}' \rangle_{\Gamma_h} \\ &+ (\sigma \partial_t \boldsymbol{a}\ ,\boldsymbol{a}')_{\Omega_{\mathrm{c}}} + (\sigma \mathbf{grad}\ v\ ,\boldsymbol{a}')_{\Omega_{\mathrm{c}}} = 0, \\ \forall \boldsymbol{a}' &\in \tilde{S}_{e0}^1, \text{ and} \end{aligned} \tag{8}$$

$$\begin{aligned} (\sigma \partial_t \boldsymbol{a}\ ,\mathbf{grad}\ v')_{\Omega_{\mathrm{c}}} &+ (\sigma \mathbf{grad}\ v\ ,\mathbf{grad}\ v')_{\Omega_{\mathrm{c}}} \\ &- \sum_{i \in C} I_i \mathcal{V}_i(v') = 0, \quad \forall v' \in S_{e0}^0, \end{aligned}$$

with $\mathcal{V}_i(v) = V_i$. For example, when $v' = v_i$ is chosen ($i \in C_I$, $V_i' = 1$), one obtains the circuit equation

$$(\sigma \partial_t \boldsymbol{a}\ ,\mathbf{grad}\ v_i)_{\Omega_{\mathrm{c}}} + (\sigma \mathbf{grad}\ v\ ,\mathbf{grad}\ v_i)_{\Omega_{\mathrm{c}}} = I_i. \tag{9}$$

The formulation (8) is referred to as the generalized modified vector potential formulation, or a-formulation. It is a weak form of Ampere's equation. The continuity of the normal component of $\boldsymbol{b}$ is enforced by the considered shape functions while the natural constraints, $\boldsymbol{h} \times \boldsymbol{n}|_{\Gamma_h}$ and I_i for $i \in C_I$ are weakly imposed.

Note that it is also possible to define v everywhere in the conducting region (instead of defining it only in a transition layer) and extend the gauge condition for $\boldsymbol{a}$ to Ω_{c} as well. In all tested situations, solutions obtained with this a-v-formulation are identical to those obtained with the a-formulation.

In practice, the a-formulation can be solved in one of two ways. Either the total vector potential $\boldsymbol{a}$ is considered as the unknown, leading to the total a-formulation, or $\boldsymbol{a}$ is decomposed into a known source potential $\boldsymbol{a}_{\mathrm{s}}$ and an unknown reaction potential $\boldsymbol{a}_{\mathrm{r}}$, $\boldsymbol{a} = \boldsymbol{a}_{\mathrm{s}} + \boldsymbol{a}_{\mathrm{r}}$, leading to the reaction a-formulation.

We now turn to 2D geometries with the current density along the invariant direction. Now, $\mathbf{grad}\ v$ is perpendicular to the plane and constant in each conducting domain [26]. The vector potential is chosen in the same direction so that the Coulomb gauge is implicit (div $\boldsymbol{a} = 0$). Fields $\boldsymbol{a}$ and $\mathbf{grad}\ v$ are discretized with Whitney elements as follows:

$$\boldsymbol{a} = \sum_{n \in \Omega} a_n\ \boldsymbol{\psi}_n \quad \text{and} \quad \mathbf{grad}\ v = \sum_{i \in C} U_i \boldsymbol{z}_i, \tag{10}$$

with $\boldsymbol{\psi}_n$ a perpendicular edge function associated to node n and $\boldsymbol{z}_i$ a piecewise-constant shape function, nonzero in $\Omega_{\mathrm{c},i}$ only. Coefficients a_n and U_i (voltage per unit length) are the degrees of freedom. The resulting formulation is analogous to formulation (8), but with the different function spaces and unknowns described in (10).

C. Time Integration

The spatial discretization yields a semi-discrete nonlinear system of equations. To obtain a fully discrete system that can be solved numerically, time must also be discretized. In this work, an implicit Euler method has been chosen. From the initial solution at time $t = t_0$, the solution is successively sought at discrete time instants $t_1, t_2, \ldots, t_{\mathrm{f}}$, not necessarily equidistant. In the equation for time t_n, $n \in \mathbb{N}_0$, all terms are

evaluated at t_n, with the time derivative of any quantity u at time t_n being approximated by the finite difference

$$\left.\frac{du}{dt}\right|_{t_n} \approx \frac{u(t_n) - u(t_{n-1})}{t_n - t_{n-1}}. \qquad (11)$$

D. Iterative Techniques

After complete discretization, the original problem takes the form of a system of nonlinear algebraic equations,

$$\mathbf{A}(\boldsymbol{x})\boldsymbol{x} = \boldsymbol{b}, \qquad (12)$$

where $\boldsymbol{x}$ is the vector of degrees of freedom at the considered time step. This nonlinear system cannot be solved directly and iterative techniques are necessary.

In this work, we consider Picard and Newton-Raphson iterative techniques.

a) The Picard technique: The Picard technique [27] belongs to fixed point methods. From an iterate $\boldsymbol{x}_i$, the next iterate $\boldsymbol{x}_{i+1}$ is sought by solving the linear system,

$$\mathbf{A}(\boldsymbol{x}_i)\boldsymbol{x}_{i+1} = \boldsymbol{b}, \quad i = 0, 1, \dots. \qquad (13)$$

In general, this method does not exhibit a high convergence rate. However, even if in some cases the iterates may enter cycles and fail to converge, this is usually a robust method in the sense that it converges for a wide range of initial guesses $\boldsymbol{x}_0$. An illustration of one iteration of this method in the case of a single unknown is given in Fig. 2a.

b) The Newton-Raphson technique: The Newton-Raphson technique [27] consists in approximating the nonlinear term $\mathbf{A}(\boldsymbol{x})\boldsymbol{x}$ to first order with a limited Taylor development, yielding a linear system. From an iterate $\boldsymbol{x}_i$, the next iterate $\boldsymbol{x}_{i+1}$ is computed by solving the following linear system,

$$\mathbf{A}(\boldsymbol{x}_i)\boldsymbol{x}_i + \mathbf{J}(\boldsymbol{x}_i)(\boldsymbol{x}_{i+1} - \boldsymbol{x}_i) = \boldsymbol{b}, \quad i = 0, 1, \dots, \qquad (14)$$

with $\mathbf{J}$ the Jacobian matrix defined by

$$\mathbf{J}(\boldsymbol{x}) = \frac{\partial}{\partial \boldsymbol{x}}\left(\mathbf{A}(\boldsymbol{x})\boldsymbol{x}\right). \qquad (15)$$

The Jacobian matrix can be evaluated numerically using finite differences but if the analytical expression of the matrix is known, it can be used. This is the case in this work. The involved analytical expressions are given in the appendix.

This method is usually less robust than the Picard technique in the sense that if the initial iterate is not *sufficiently close* to the solution, the method may diverge. However, when the initial guess is sufficiently close to the solution the convergence can be very fast, with a quadratic rate of convergence. An example of one iteration of this method in the case of a single unknown is given in Fig. 2b.

c) Choosing the initial guess: Iterations must start with an initial guess, or a predictor. The simplest possibility is to consider the solution at the previous time step. This method is referred to as the zeroth-order extrapolation method. Several previous solutions can also be extrapolated and a class of polynomial extrapolation methods can be defined. In this work, we consider extrapolations up to order two (that involves the solution at the last three time steps).
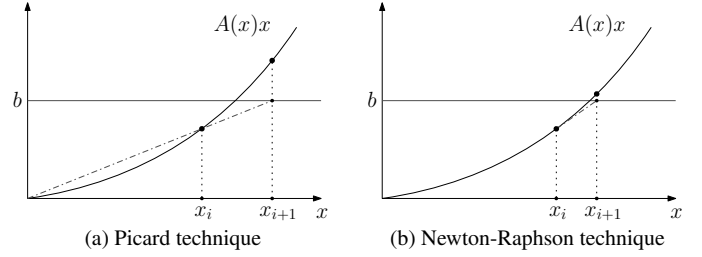

Fig. 2: One iteration of the Picard and Newton-Raphson iterative techniques in the case of a single degree of freedom.

III. COMPARISON OF THE METHODS

The comparison of the different methods is conducted progressively. First, the application of the iterative techniques on the nonlinear laws is analyzed in a case with a single-degree-of-freedom. As shown below, the conclusions drawn in the simple case extend to 1D, 2D and 3D problems. Then, the accuracy of the different methods is evaluated and their efficiency is compared in two benchmarked 2D problems. Finally, the methods are illustrated on a benchmarked 3D problem.

In this section, no magnetic material is considered and $\boldsymbol{b} = \mu_0 \boldsymbol{h}$ everywhere in the domain. Simulations are performed by the GetDP free software [28], [29] and meshes are generated by Gmsh [30]. Model files for the main test cases are available on the website www.life-hts.uliege.be.

A. Behavior of the Iterative Techniques

An important difference between the h- and a-formulations is that they involve the nonlinear electric constitutive law in a different manner, either through the electrical resistivity or the electrical conductivity. The shape of this constitutive law has a strong influence on the behavior of the iterative techniques, as we now illustrate for simple equations with a single unknown.

Consider a superconducting ring subjected to a time-varying external magnetic flux $\dot{\Phi}$. The ring can be modelled by lumped elements: a nonlinear resistor $R = V_c/I_c(|I|/I_c)^{n-1}$, that mimics the electrical resistivity law, in series with a linear inductor L, yielding $R(I)I + L\dot{I} = \dot{\Phi}$. Solving the problem for the current intensity I flowing in the ring gives rise to an equation of the form (after time discretization) $f(x) = |x|^{n-1}x + x = b$, to be solved at each time step. By contrast, solving for the voltage across the modeling resistor gives rise to an equation of the form $f(x) = |x|^{(1-n)/n}x + x = b$. The shape of f in both cases is depicted in Fig. 3. The first case is analogous to the h-formulation because it involves a resistivity-like parameter whereas the second one is analogous to the a-formulation with a conductivity-like component.

Applying the iterative techniques on the two nonlinear shapes yields the following results. The first equation, $f(x) = |x|^{n-1}x + x = b$ (h-formulation), is more efficiently solved with the Newton-Raphson technique, as the Picard iterations easily cycle and fail to converge. An example of cycle is shown in Fig. 4a. Conversely, the second equation, $f(x) = |x|^{(1-n)/n}x + x = b$ (a-formulation), can hardly be
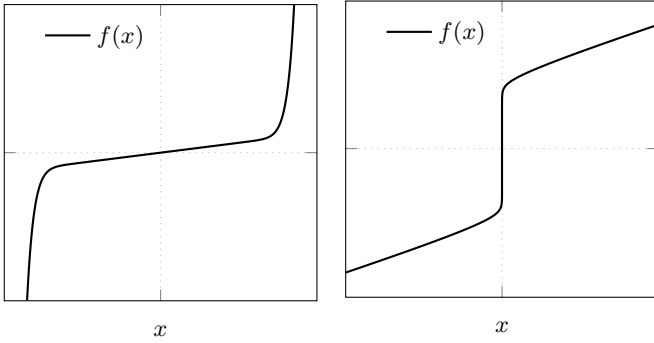
(a) $f(x) = x^n + x$ (h-form.).   (b) $f(x) = x^{1/n} + x$ (a-form.).

Fig. 3: Typical shape of the nonlinear functions encountered with the h-formulation (a) and with the a-formulation (b).

solved with the Newton-Raphson technique whereas the Picard technique shows a good stability. With the Newton-Raphson technique, iterations also enter cycles as illustrated in Fig. 4b. Note that for each case in Fig. 4, the cycling behavior can be circumvented by using relaxation factors, which however requires several trials to determine the most efficient values to be used.
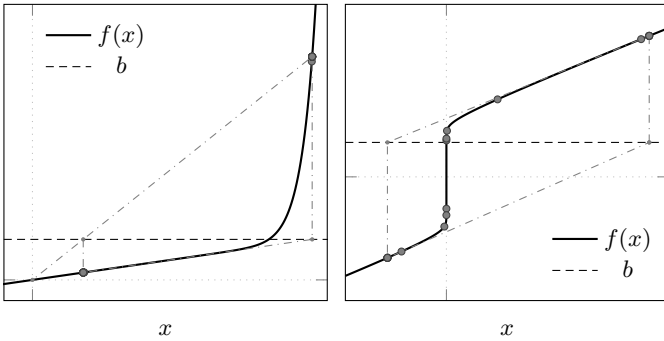
(a) Picard and h-formulation.   (b) N-R and a-formulation.

Fig. 4: Illustration of iteration cycles encountered when solving the superconducting ring problem. Gray dots represent the successive iterates and dash-dotted lines connect two successive iterations. N-R stands for Newton-Raphson.

As shown below, the observed behaviors can be generalized to 1D, 2D and 3D problems: the Picard technique does not work directly with the h-formulation whereas the Newton-Raphson technique fails to converge when used to linearize the a-formulation. The origin of the corresponding convergence issues was observed to be identical to that in the above simple problems, as in some regions of the mesh, the degrees of freedom enter cycles. Again, it is sometimes possible to overcome these cycles by using finely tuned relaxation factors, a method which however requires trial-and-error.

B. Comparison of 2D Models

The numerical study is conducted on two different problems. The first problem consists in a superconducting bulk cylinder subjected to an external applied field. The geometry is axisymmetric and only one slice of one radian is modelled.

This test case will be referred to as the *bulk* case and is comparable to benchmark 4 of the HTS modeling website [16].

The second problem consists in a superconducting thin tape transporting an imposed AC current intensity. The geometry is assumed two-dimensional and only the cross-section of the tape of modelled. This test case will be referred to as the *tape* case and is comparable to benchmark 1 of the HTS modeling website [16].

Following the conclusions of the previous section, the h-formulation is solved with the Newton-Raphson technique whereas the a-formulation is solved with the Picard technique.

a) Convergence criterion: The chosen convergence criterion for the iterative techniques is based on an estimate P of the instantaneous electromagnetic power. For the h-formulations, P is expressed as

$$P = \left(\partial_t(\mu\, \boldsymbol{h})\,, \boldsymbol{h}\right)_\Omega + \left(\rho\, \boldsymbol{j}\,, \boldsymbol{j}\right)_{\Omega_c}, \tag{16}$$

with $\boldsymbol{j} = \mathbf{curl}\, \boldsymbol{h}$. For the a-formulations, P is given as

$$P = \left(\nu\, \partial_t \boldsymbol{b}\,, \boldsymbol{b}\right)_\Omega + \left(\sigma \boldsymbol{e}\,, \boldsymbol{e}\right)_{\Omega_c}, \tag{17}$$

with $\boldsymbol{b} = \mathbf{curl}\, \boldsymbol{a}$ and $\boldsymbol{e} = -\partial_t \boldsymbol{a} - \mathbf{grad}\, v$.

The criterion requires the relative change[1] of P between two iterations to be smaller than a given tolerance ε. This choice of convergence criterion is motivated by the observation that similar residuals do not correspond to similar accuracies in each formulations whereas quantity P is comparable between the formulations.

In the following, we first evaluate the accuracy of the numerical solutions. Then, we compare the efficiency of the methods that lead to accurate results.

1) Accuracy of the formulations:

Bulk case: The bulk superconductor has a radius $R = 12.5$ mm and a height $H = 10$ mm. The critical current density is $j_c = 3 \times 10^8$ A/m^2. Cylindrical coordinates (r, θ, z) are introduced. The cylinder is subjected to an external field applied parallel to its axis (the z-axis), so that the problem is axisymmetric. The time evolution of the applied field is illustrated in Fig. 5 with $b_{max} = 1$ T and t_1, t_2, and t_3 equal to 5, 10, and 15 s, respectively.
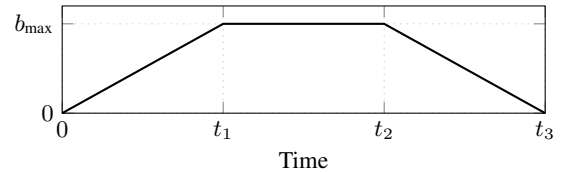

Fig. 5: Time evolution of the external applied field in the bulk test case.

Fig. 6 shows the azimuthal current density obtained with both formulations at the three instants t_1, t_2, and t_3, whereas Fig. 7 shows the corresponding vertical components of the magnetic flux density 2 mm above the cylinder. With mesh and time refinement, the solutions of the h- and a-formulations

---

[1]The relative change is defined as $|(P_i - P_{i-1})/P_{i-1}|$, with P_i the value of the convergence indicator at iteration i. If the value of P_{i-1} is smaller than 10^{-7}, the relative change is replaced by the absolute increment divided by 10^{-7} W/m. This scheme is followed to avoid convergence issues when P_{i-1} is too small and is only motivated by the tested situations.

are seen to approach each other (both globally and locally). The global convergence is illustrated in Fig. 8.
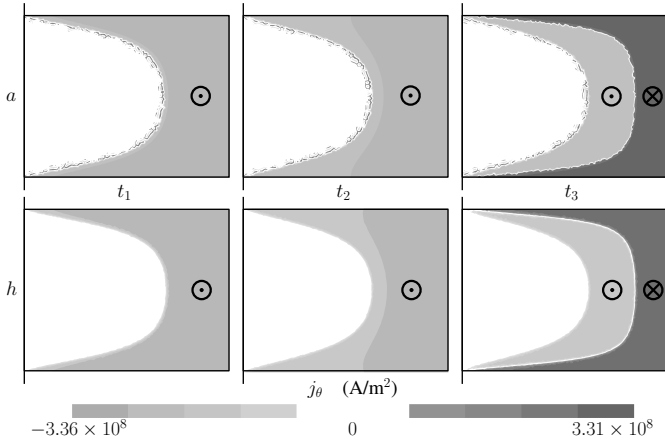

Fig. 6: Current density distribution in a slice of the bulk cylindrical geometry at the instants t_1, t_2 and t_3 for a maximum applied field of 1 T and $n = 20$. White areas are free of current, light gray areas are crossed by out-of-plane current densities and dark gray areas are crossed by opposite current densities. Top: a-formulation. Bottom: h-formulation.
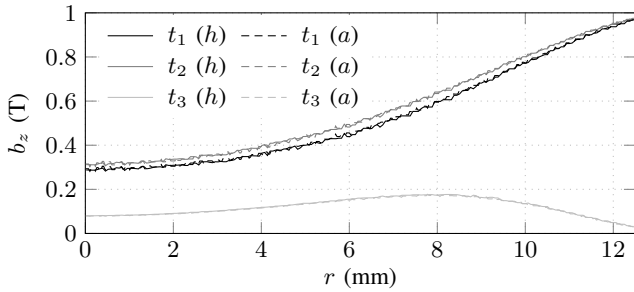

Fig. 7: Distribution of the z-component of the magnetic flux density 2 mm above the cylinder at the instants t_1, t_2 and t_3 for a maximum applied field of 1 T and $n = 20$. Solid lines: h-formulation. Dashed lines: a-formulation.
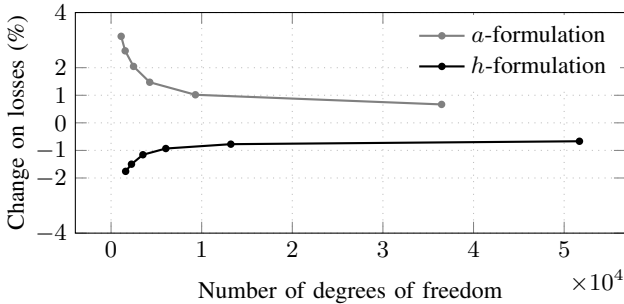
Fig. 8: Change of AC losses $\oint_{\text{cycle}} (\boldsymbol{j}, \boldsymbol{e})_{\Omega_c} \, dt$, relative to an accurate solution, for various numbers of spatial degrees of freedom, for the two formulations, with constant time step ($\Delta t = t_1/50$ s), and $n = 25$. The reference value is determined as the arithmetic mean of the solutions obtained with the finest mesh, in the h- and a-formulations (4.9495 J/m·cycle).

Note that the quality of the solution is not always good for coarser meshes and/or large time steps. For instance, the fields

$\boldsymbol{h}$ obtained with the h-formulation and $\boldsymbol{a}$ obtained with the a-formulation both exhibit *small* amplitude oscillations over a few elements, located ahead of the sharp flux penetration front. This results in oscillations in the other fields also. Because the current density is expressed through the power law in the a-formulation, the oscillations are strongly amplified. In the h-formulation, the current density is obtained through the curl of $\boldsymbol{h}$ and the oscillations are thus not as much amplified, as shown in Fig. 9. In both formulations, the error is localized in a few elements and thus becomes negligible when the mesh is refined (see the lower part of Fig. 9, and also Fig. 6). As discussed below, the choice of the time step also has an important influence on the solution accuracy.
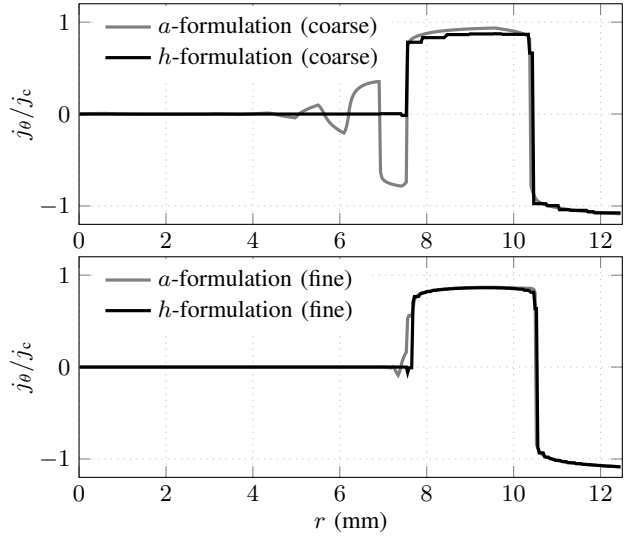

Fig. 9: Current density profiles, as a function of the distance r to the symmetry axis, at the mid-height of the cylinder, at time t_3 for a maximum applied field of 1 T and $n = 20$. Upper figure: coarse mesh of 1661 nodes. Lower figure: finer mesh with 36989 nodes.

Tape case: The tape has a large aspect ratio: its height is $H = 1$ μm and its width is $W = 12$ mm. The critical current density is $j_c = 2.5 \times 10^{10}$ A/m^2. Cartesian coordinates are introduced with the x-axis along the width of the tape and the y-axis along its height. A sine-wave current intensity $I(t) = I_{\max} \sin(2\pi f t)$ is imposed, with a frequency $f = 50$ Hz and an amplitude $I_{\max} = F I_c$, where $I_c = H W j_c$ is the critical current intensity and $F \in [0, 1]$ a constant. The superconducting domain is meshed with one layer of first-order quadrangular elements.

Fig. 10 shows the current density and magnetic flux density distributions after one fourth of a period obtained with both formulations. Again, with mesh and time refinement, the solutions of the h- and a-formulations converge to each other and the solutions are reliable, see Fig. 11. Note that the current density profile is still very sensitive to the $\boldsymbol{a}$ field with the a-formulation, especially with large n values. The convergence criterion must be strong enough if accurate current density profiles are sought with the a-formulation.

Reaction and total formulations: The solutions above were obtained with the total h- and a-formulations. Numerical solutions of the *reaction* formulations are exactly identical to
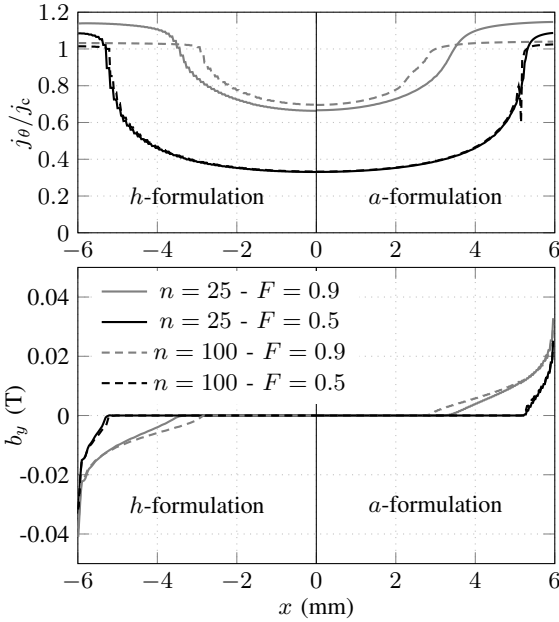
Fig. 10: Current density and magnetic flux density distributions in the tape at time instant $1/(4f)$ for different power exponents n and imposed current intensities $I_{\max} = F I_c$. Left: h-formulation. Right: a-formulation.
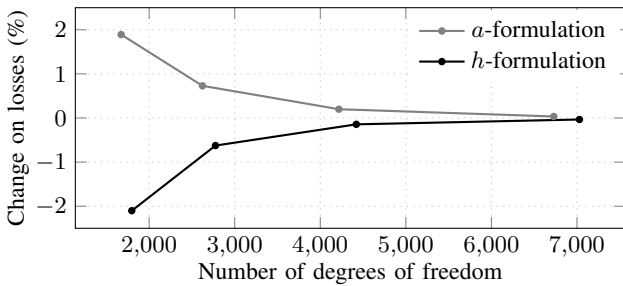

Fig. 11: Change of AC losses $\oint_{\text{cycle}} (\boldsymbol{j}, \boldsymbol{e})_{\Omega_c} \, dt$, relative to an accurate solution, for various numbers of spatial degrees of freedom, for the two formulations, with constant time step ($\Delta t = 1/(50f)$ s), and $n = 100$. The accurate solution is the arithmetic mean of the values obtained with the finest mesh, in the h- and a-formulations.

those of the total formulations. Of course, this is only the case provided that the source field $\boldsymbol{h}_s$ or potential $\boldsymbol{a}_s$ are representable in the corresponding shape function space.

Influence of the time step: The choice of the time step is important for both the solution accuracy and the convergence properties. The motivation for studying this influence is based on the observation that, in some situations, the iterative techniques converge even with very large time steps, while providing reliable magnetic flux density distributions. With the a-formulation and the Picard linearization technique, it has even been observed that the larger the time step, the easier the convergence. A single-time-step method has already been discussed by Lousberg in [11], [18]. To some extent, such an approach is also possible with the h-formulation and the Newton-Raphson technique. It is thus tempting to use very large time steps to accelerate the simulations. This possibility should however be exploited with care as not all quantities are

reliable when large time steps are used.

To check the validity of the results, a simple one-dimensional case is considered. It consists in a 25-mm-wide slab subjected to a parallel field increasing linearly over time at 5 T/s. Note that in the limit of fine meshes and small time steps, both h- and a-formulations accurately reproduce the analytical results of [31]. Magnetic flux and current penetration profiles are compared for two time discretization levels: with a single-time-step, and with 100 time steps. Materials with $n = 10$ and $n = 100$ are chosen. Fig. 12 compares the corresponding numerical solutions for the h-formulation. Results from the a-formulation are similar. As can be seen in the figure, even if the method has converged in the four cases, there is a large error on the magnetic flux density distribution and the current density profile for the low power exponent $n = 10$. Clearly, the single-time-step approach is not reliable in that case. However, with a larger exponent, both time discretization levels provide accurate results.
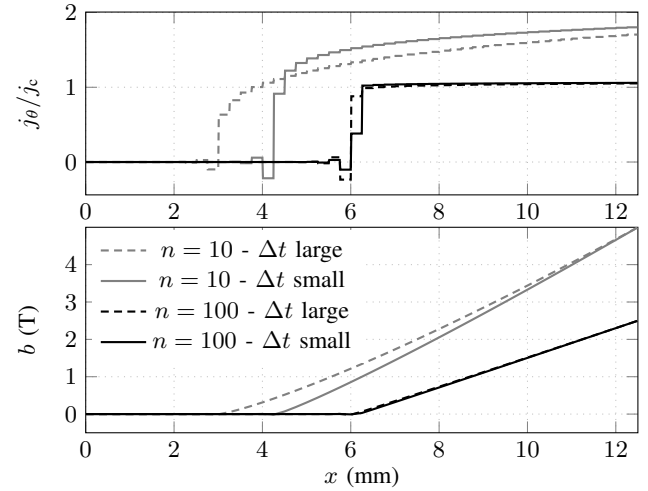

Fig. 12: Comparison between the numerical solutions for two time discretization levels for $n = 10$ and $n = 100$. Dashed curves correspond to the solution obtained with a single time step whereas solid curve are obtained after 100 time steps. Solid curves coincide with the approximated analytical solution from [31] (not represented in the figure). Solutions of the h-formulation, in a 1D geometry. Applied field rate: 5 (T/s).

These observations can be explained as follows. In the Bean model [32] limit ($n \to \infty$) and with a linear ramp of applied field, the magnetic flux density distribution is linear in space and the flux front propagates at constant speed. In the finite element model, time derivatives are estimated by a finite difference approximation (backward Euler method). This approximation amounts to replacing the instantaneous increase of the magnetic flux density by its *average* increase over the considered time step. This is illustrated in Fig. 13 in the extreme case of a single time step for the whole time interval, for a magnetization from a virgin state. In this situation, the time derivative is *underestimated* almost everywhere in the material. If more time steps are considered, the underestimation error is localized near the front and its influence is thus reduced. A power law model with a finite exponent n yields a different distribution but the finite difference still underestimates the

time derivative. The error on the time derivative is present both for small values of n and in the Bean limit. However, the effect of this error on the current and flux distributions is found to be larger for smaller n, as previously observed in [11].
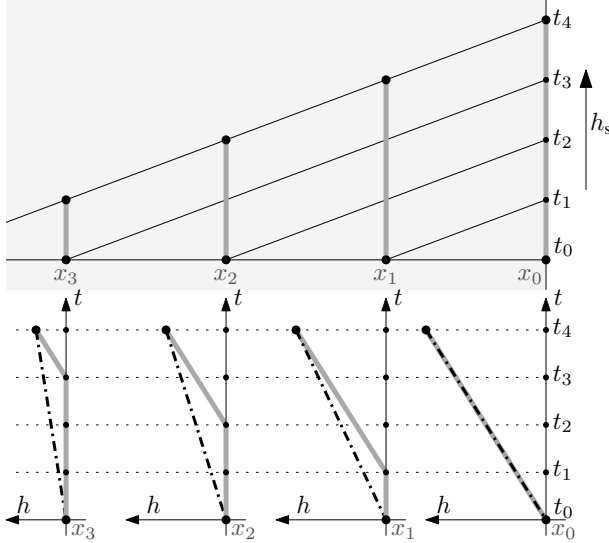

Fig. 13: Illustration of the error induced by the finite difference approximation of the time derivative in the case of large time steps. Up: inside the superconductor, magnetic flux density distribution at several time instants for a linearly increasing source field in the Bean model limit. Down: time evolution of the magnetic flux density at several spatial points (bold gray curves) and illustration of the finite difference approximation (dash-dotted lines) in the case of a single numerical time step. Time instants $t_0, \ldots, t_4$ are equidistant.

The error on time derivatives induces an error on $\boldsymbol{e}$ (via Faraday's law $\mathbf{curl}\ \boldsymbol{e} = -\partial_t \boldsymbol{b}$ in the h-formulation and via $\boldsymbol{e} = -\partial_t \boldsymbol{a} - \mathbf{grad}\ v$ in the a-formulation). With large n, the resulting error on $\boldsymbol{j}$ is small because of the strong nonlinearity of the constitutive law. For decreasing n, the sensitivity of $\boldsymbol{j}$ to $\boldsymbol{e}$ increases for $\|\boldsymbol{j}\|$ close to j_c and the error on $\boldsymbol{j}$ thus increases. Because $\boldsymbol{e}$ is underestimated, $\boldsymbol{j}$ is also underestimated and, to reach $\boldsymbol{h} = \boldsymbol{h}_s$ at the material-air interface, this implies a larger penetration distance, as observed in the simulations. Therefore, even though the use of very large time steps provides accurate current and field distributions when n is large enough, time derivatives are always underestimated and this leads to non-negligible errors on the electric field. Power quantities and losses rely on time derivatives and are thus also underestimated. The use of large time steps is thus not appropriate for computing the instantaneous power dissipation or losses.

Conclusions on the accuracy: All formulations lead to accurate and reliable results provided that the time step, the mesh size, and the convergence criterion are sufficiently small. For coarser meshes, the a-formulation provides large oscillations of the current density in non-penetrated regions. There is a possibility to use large time steps to speed up the simulations, more specifically in the a-formulation, but the accuracy on time derivatives is reduced. This can nevertheless be exploited to obtain fast and reliable magnetic flux density

and current distributions for large n.

2) Efficiency of the formulations: The convergence speed of all methods is not identical. Depending on the method and on the choice of the first iterate, or predictor, the iterative techniques may require very different numbers of iterations to converge. Because the simulation time is proportional to the total number of iterations, this affects the calculation speed. The accurate methods which were identified in the previous section (small time step, fine mesh, and strong convergence criterion) are now compared in terms of their efficiency.

To proceed, the bulk and the tape cases are considered with three discretization levels: coarse, medium, and fine, defined by a multiplier α equal to 4, 2, and 1, respectively. The power law exponent is $n = 25$ in both geometries and $F = 0.9$ for the tape. In the bulk case, the mesh size varies from 0.3α mm in the cylinder to 3α mm at the outer surface. The number of time steps from 0 to t_3 is $300/\alpha$. In the tape case, the number of quadrangular elements along the width of the tape is $400/\alpha$ and the number of time steps for one period is $100/\alpha$.

In some situations, the iterative techniques diverge or do not converge in a reasonable number of iterations. To treat automatically these issues, an adaptive time step procedure is implemented. This is crucial for efficient resolutions with the Newton-Raphson technique: small time steps are typically necessary during the first penetration of magnetic flux but one can afford larger steps once the sample is saturated. The heuristic procedure is defined as follows (procedure from [33]): (1) if the number of iterations exceeds $i_{\max}$ with a time step Δt or if the iteration diverges, the current time integration step restarts with a smaller time step equal to $\gamma \Delta t$, with $\gamma < 1$, (2) if a step with time step Δt converges in less than i_{fast} iterations, the next time step is chosen equal to $\min(\beta \Delta t, \Delta t_{\max})$, with $\beta > 1$ and a fixed $\Delta t_{\max}$. Here, we choose $\gamma = 1/2$, $\beta = 2$, $\Delta t_{\max}$ equal to the initial time step, $i_{\text{fast}} = i_{\max}/4$. For the h- and a-formulations, we choose $i_{\max} = 60$ and $i_{\max} = 500$, respectively.

Table I shows the number of solved linear systems required in the bulk and tape cases, with the two formulations and different extrapolation orders for the first iterate. Clearly, for an identical time discretization, the slower convergence rate of the Picard technique used in the a-formulation is detrimental and the h-formulation is more efficient. This can be observed in Fig. 14, where the system residual does not decrease monotonously with the Picard technique whereas a quadratic convergence rate is obtained at the last iterations with the Newton-Raphson technique.

Results show that choosing the first iterate (the predictor) with an extrapolation from the previous time steps is efficient for reducing the total number of iterations. A good choice is the first-order extrapolation of the last two steps with the h-formulation and the second-order extrapolation of the last three steps for the a-formulation.

If a good accuracy is sought for all quantities, small time steps should be used and, in that case, the h-formulation reaches a solution faster. Typically, with identical discretization levels, the h-formulation is two to ten times faster than the a-formulation. On the contrary, in controlled situations where the use of large time steps is acceptable, e.g., with large n

Formulation	Total h			Total a		
Linearization	Newton-Raphson			Picard		
Extrapolation	0th	1st	2nd	0th	1st	2nd
Bulk Coarse	570	612	824	16382	10905	9182
Bulk Medium	1287	1344	1808	34858	20935	16654
Bulk Fine	2671	2751	3780	74929	41467	27006
Tape Coarse	4124	836	455	2551	2338	1827
Tape Medium	8558	983	732	5665	5001	4222
Tape Fine	17266	867	1058	13628	12039	8172

TABLE I: Total number of solved linear systems for the simulation from 0 to t_3 in the bulk case and for $5/4f$ in the tape case, for three discretization levels, three extrapolation techniques with the h-formulation and the a-formulation. Relative tolerance for the convergence criterion: 10^{-6} (except for the tape with the a-formulation, 10^{-4}). Simulation times for the fastest simulations of each line are, on a single Intel Xeon 2 GHz CPU with 4Gb RAM, from top to bottom, 12s, 1m55s, 1h38m, 20s, 2m50s, and 14m.
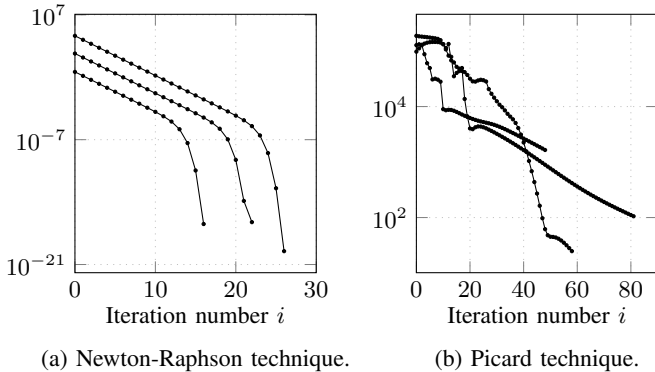

(a) Newton-Raphson technique. (b) Picard technique.

Fig. 14: Evolution of the 2-norm of the residual $r_i = b - \mathbf{A}(x_i)x_i$ with the iterations, for three examples of time integration step and for the two linearization techniques, for the bulk case. (a) Newton-Raphson with the h-formulation and the zeroth-order extrapolation. (b) Picard with the a-formulation and the first-order extrapolation.

values and for determining the current and flux distributions, the a-formulation is much more stable and might be used to get fast results, as will be illustrated in the next section. In that case of large time steps, the h-formulation with the Newton-Raphson technique is less appropriate because the iterations diverge if the initial estimate is not sufficiently close to the solution.

C. Cube 3D Model

The conclusions shown above are now illustrated on a 3D problem: a superconducting cube subjected to an external applied field parallel to its side faces. The problem is similar to benchmark 5 of the HTS modeling website [34]. The cube side is $a = 10$ mm, materials properties are $j_c = 10^8$ A/m^2 and $n = 100$. The applied field is homogeneous and varies sinusoidally with time with a peak value of 200 mT and a frequency $f = 50$ Hz. One eighth of the cube is modelled. The superconducting domain is meshed with cubes ($16 \times 16 \times 16$ cubes) and the surrounding domain is meshed with tetrahedra and pyramids.

The magnetization curve is computed by two methods: the a-formulation with large time steps (20 steps only for the curve, calculation time 3h30m, same CPU as in Table

I) for a fast resolution, and the h-formulation with smaller time steps (300 steps for the curve, calculation time 10h) for an accurate evaluation of all quantities. The magnetization curves are given in Fig. 15, they both match the benchmark results. Even for large time steps, the a-formulation yields accurate magnetization values, due to the large n-value. On the contrary, to compute accurately time integrated quantities, it is necessary to use smaller time steps. In that case, the h-formulation is recommended. For illustration, a perspective view of the solution of both formulations is given in Fig. 16. Again, note the slight oscillations of the current density after the flux front from the a-formulation. If needed, these oscillations can be decreased by refining the mesh and strengthening the convergence criterion.
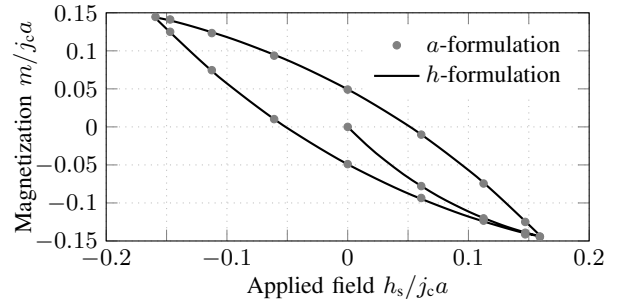

Fig. 15: Magnetization curve for the superconducting cube, obtained with two formulations. Gray dots represent the solutions at successive (large) time steps.
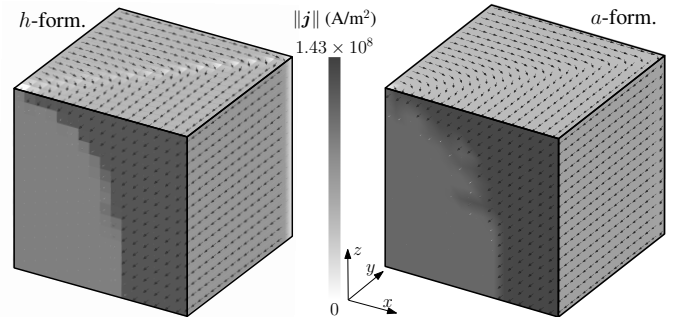

Fig. 16: Current density distribution on the boundaries of one eighth of the superconducting cube after the first ramp of $\mu_0 h_s = 0.2$ T. Left: h-formulation. Right: a-formulation. Scale is for the arrow color.

IV. EXTENSION TO SYSTEMS CONTAINING SOFT FERROMAGNETS

The models developed above are directly adapted for treating systems containing *linear* isotropic non-conducting ferromagnetic domains. To model saturation, a nonlinear law must be introduced and an appropriate linearization technique must be chosen. It appears that the approach followed for the superconductor can be transposed for the ferromagnet.

A simple model for an isotropic saturation law expresses the permeability $\mu = \mu(h)$ as a rational expression of first order-polynomials, leading to the following relationship:

$$b = \mu_0 \left(1 + \left(\frac{1}{\mu_{\text{r0}} - 1} + \frac{\|h\|}{m_0}\right)^{-1}\right) h, \qquad (18)$$

with $\mu_{\mathrm{r}0}$ the relative permeability at origin and m_0 (A/m) the saturation magnetic field. A graphical representation of this law is given in Fig. 17. The permeability law is involved in the h-formulation. The model can be explicitly inverted (see the appendix) to yield the reluctivity law required for the a-formulation.
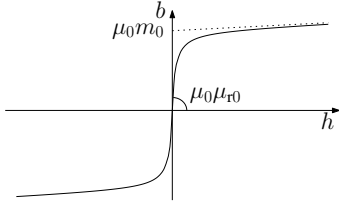

Fig. 17: Ferromagnetic constitutive law and representation of the physical parameters.

The behavior of the iterative techniques on this nonlinear law is found to be analogous to what was observed for the power law. On the one hand, the law $\boldsymbol{b} = \mu \boldsymbol{h}$ has the same concavity than the law $\boldsymbol{j} = \sigma \boldsymbol{e}$ and the application of the Newton-Raphson technique leads to iteration cycles, although the situation is less severe here because the permeability is finite at the origin. On the other hand, the law $\boldsymbol{h} = \nu \boldsymbol{b}$ is comparable to the law $\boldsymbol{e} = \rho \boldsymbol{j}$ and, in that case, the Picard technique is less appropriate.

Following the same reasoning as with the superconductor, it is therefore recommended to linearize the h-formulation with a Picard technique and the a-formulation with a Newton-Raphson technique when modeling soft ferromagnets only. The a-formulation is thus expected to be more efficient than the h-formulation because it will benefit from the high rate of convergence of the Newton-Raphson technique. This is what is actually observed. Note that we also found that switching from the Picard technique to the Newton-Raphson technique for $\boldsymbol{b} = \mu \boldsymbol{h}$ after a given number of iterations also helps avoiding cycles. This however remains less efficient than using the a-formulation.

Remarkably, conclusions for the superconductor and the ferromagnet are antagonistic: the h-formulation is preferred for the former material whereas the a-formulation is more efficient for the latter. Using a single formulation for the whole domain is thus expected to be sub-optimal. Consequently, we investigated the benefits of using a coupled formulation in a 2D example.

A. Coupled Formulation

Let the problem domain Ω be decomposed into two parts: $\bar{\Omega}$ containing the superconducting domain and its boundary and $\hat{\Omega}$ containing the union of the ferromagnetic, the air (or cryogenic fluid) domains, and their boundaries. Thus, $\bar{\Omega} \cup \hat{\Omega} = \Omega$. Their non-empty intersection $\bar{\Omega} \cap \hat{\Omega}$ is a curve and is denoted by Γ_{m}, as illustrated in Fig. 18 (note that $\bar{\Omega}$ must not necessarily be enclosed by $\hat{\Omega}$). Surfaces $\bar{\Gamma}_e$, $\bar{\Gamma}_h$, $\hat{\Gamma}_e$ and $\hat{\Gamma}_h$ are defined in the associated domains. Note that the air domain could be placed in $\bar{\Omega}$ instead.

Domain $\bar{\Omega}$ is solved with the h-formulation whereas domain $\hat{\Omega}$ is solved with the a-formulation. The coupling surface
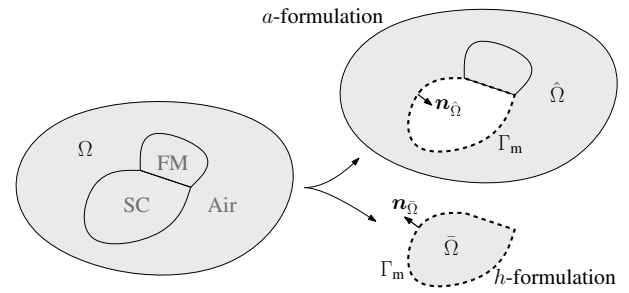

Fig. 18: Schematics of the domain decomposition for the coupled formulation. SC, FM and Air stand for the superconducting, ferromagnetic, and air (or cryogenic fluid) domains.

Γ_{m} is treated differently in the two sets; degrees of freedom on this surface cannot be known *a priori*, and thus cannot be strongly imposed. Instead, the coupling can be weakly imposed within the surface integrals in the weak formulations, as natural continuity constraints. Consequently, $\Gamma_{\mathrm{m}} \subset \bar{\Gamma}_e$ and $\Gamma_{\mathrm{m}} \subset \hat{\Gamma}_h$. It can be shown that this procedure weakly ensures the continuity of the tangential component of $\boldsymbol{h}$ and of the normal component of $\boldsymbol{b}$.

For conciseness, let $\bar{\Gamma}_e$ and $\hat{\Gamma}_h$ be equal to Γ_{m}. The coupled formulation is then expressed as follows:

From an initial solution at time $t = 0$, find $\boldsymbol{h} \in \bar{S}_h^1(\bar{\Omega})$ and $\boldsymbol{a} \in \tilde{S}_e^1(\hat{\Omega})$ such that, for $t > 0$,

$$\left(\partial_t(\mu\, \boldsymbol{h})\,, \boldsymbol{h}'\right)_{\bar{\Omega}} + \left(\rho\, \mathbf{curl}\, \boldsymbol{h}\,, \mathbf{curl}\, \boldsymbol{h}'\right)_{\bar{\Omega}_{\mathrm{c}}}$$
$$+ \left\langle \partial_t \boldsymbol{a} \times \boldsymbol{n}_{\bar{\Omega}}\,, \boldsymbol{h}'\right\rangle_{\Gamma_{\mathrm{m}}} + \sum_{i \in C} V_i \mathcal{I}_i(\boldsymbol{h}') = 0, \quad (19)$$

$$\left(\nu\, \mathbf{curl}\, \boldsymbol{a}\,, \mathbf{curl}\, \boldsymbol{a}'\right)_{\hat{\Omega}} - \left\langle \boldsymbol{h} \times \boldsymbol{n}_{\hat{\Omega}}\,, \boldsymbol{a}'\right\rangle_{\Gamma_{\mathrm{m}}} = 0,$$

$$\forall \boldsymbol{h}' \in \bar{S}_{h0}^1(\bar{\Omega}) \text{ and } \forall \boldsymbol{a}' \in \tilde{S}_{e0}^1(\hat{\Omega}).$$

Note that the coupling operates through the two surface integral terms. Similar coupling schemes are discussed in detail in [35] and [36], and have been introduced in another context in [37].

B. Efficiency Comparison

The benefits of using the coupled formulation are illustrated on an induced current case. The geometry consists in a ferromagnetic cylinder ($\mu_0 m_0 = 1.31$ T, $\mu_{\mathrm{r}0} = 1700$) of radius $R = 12.5$ mm and height $H_{\mathrm{ferro}} = 5$ mm placed on the top of a superconducting bulk cylinder ($n = 20$, $j_{\mathrm{c}} = 3 \times 10^8$ A/m^2) of radius R and height $H_{\mathrm{super}} = 5$ mm. The system is subjected to an external applied field aligned with the cylinders axis (increasing from 0 T to the maximum applied field of 5 T with a rate of 25 mT/s, then decreasing to -5 T with the opposite rate). The accuracy of the formulation is successfully verified. The efficiency is summarized in Table II for different methods and discretization levels. The mesh size varies from 0.3α mm in the cylinders to 5α mm at the outer surface, with α equal to 4, 2, and 1 in the coarse, medium and fine levels, respectively. For the coupled formulation for example, this gives rise to 840, 2800, and 10800 degrees of freedom, respectively. The minimum number of time steps is fixed to $400/\alpha$. The hybrid linearization technique consists in

switching from Picard iterations to Newton-Raphson iterations after a given number of iterations (here 20).

Materials	SC and FM					
Form.	Total h		Total a	Coupled		
Lin. SC	NR	NR	Pi	NR	NR	NR
Lin. FM	Hybrid	NR	NR	NR	NR	NR
Extr.	1st	1st	2nd	0th	1st	2nd
Coarse	*1878*	<u>*3268*</u>	4381	*1360*	**1071**	*2078*
Medium	*3366*	<u>*4083*</u>	7539	*2430*	**1931**	*3609*
Fine	*7350*	<u>*4422*</u>	14594	*5235*	**3753**	*8853*

TABLE II: Total number of solved linear systems for the loading-unloading cycle for different methods and three discretization levels. Bold numbers are the minima of each line. Underlined numbers correspond to simulations where cycles in the iterations were encountered. Italic numbers refer to simulations where the Newton-Raphson technique diverged at least once (and where the time step had to be temporarily reduced). SC stands for superconductor, FM for ferromagnet. NR stands for Newton-Raphson, Pi for Picard. Relative tolerance for the convergence criterion: 10^{-6}. Simulation times on a single Intel Xeon 2 GHz CPU with 4Gb RAM are 56s, 5m30s, and 48m40s for the bold numbers.

The first observation is that in all configurations, the coupled formulation, with first-order extrapolation, is the most efficient one.

The total a-formulation suffers from the low convergence rate of the Picard technique. Nevertheless, as already mentioned, the Picard technique in the a-formulation can still be useful when using very large time steps (not represented in the table). In that case, it becomes more stable than the Newton-Raphson technique of the h-formulation.

When the total h-formulation does not encounter iteration cycles, its efficiency is found to be nearly equivalent to that of the coupled formulation. However, there is no *a priori* guarantee that a cycle will not be encountered (in the example of Table II, cycles appear in all three cases). The time step must be sufficiently small, but no quantitative criterion has been found and if cycles arise, the number of iterations strongly increases. In the presence of a cycle, the efficiency can be improved in practice with a fine tuning of the time stepping parameters. The resulting set of parameters would however not necessarily apply to other geometries or materials. Also, using a relaxation factor procedure, e.g. an accelerated search technique [38], can help to avoid cycles. It however requires several trials to find the right factor and because better results can be obtained with other methods, this solution has not been investigated further.

The hybrid technique for linearization of the ferromagnet is interesting to prevent cycles but becomes detrimental in situations where these cycles do not appear or with finer discretizations. Again, this could be optimized by making the switching procedure more specific. Because it would also rely on a trial-and-error procedure and would not necessarily generalize to other problems, this is not desirable.

The coupled formulation is simple and robust and does not need parameter tuning.

V. CONCLUSION

In this work, we compared the accuracy and efficiency of two finite element formulations for modeling high-temperature superconductors in 1D, 2D, and 3D geometries. We concluded that the choice of the formulation essentially depends on the sought results. When accurate results are wanted, the h-formulation might be preferred, together with a Newton-Raphson linearization technique and an adaptive time step procedure. Moreover, efficiency is highly enhanced when an appropriate predictor is chosen, e.g., a linear extrapolation of the last two solutions. When one can afford less accuracy on quantities relying on time derivatives, very fast results can be obtained with the a-formulation together with the Picard linearization technique. This option is particularly interesting in the case of large exponent values in the conductivity power law to get a good approximation of the magnetic field and the current density.

We applied the same approach to soft ferromagnetic materials. We arrived at opposite conclusions, the a-formulation is the most efficient and we thus proposed a coupled formulation to model systems containing both high-temperature superconductors and soft ferromagnets.

In further works, others aspects such as thermal coupling, b-dependent j_c, anisotropic properties or ferromagnetic hysteresis would be very interesting to investigate.

APPENDIX

The linearization of the system matrix by the Newton-Raphson technique requires the expressions of the derivatives of the nonlinear constitutive laws. As these laws are vector relations, the derivatives are second-order tensor expressions. In the following expressions, index notation is used.

The superconductor constitutive relation (2) diverges for $\|\boldsymbol{e}\| \to 0$. In this work, the constitutive law has been regularized as follows,

$$\boldsymbol{j} = \frac{j_c}{e_c} \frac{1}{\varepsilon_\sigma + (\|\boldsymbol{e}\|/e_c)^{(n-1)/n}} \; \boldsymbol{e} = \sigma(\|\boldsymbol{e}\|)\boldsymbol{e}, \qquad (20)$$

with $\varepsilon_\sigma = 10^{-8}$. Its tensor derivative is given by

$$\frac{\partial j_i}{\partial e_j} = \sigma(\|\boldsymbol{e}\|) \; \delta_{ij} - \frac{n-1}{n} \frac{(\sigma(\|\boldsymbol{e}\|))^2}{j_c e_c} \left(\frac{e_c}{\|\boldsymbol{e}\|}\right)^{(n+1)/n} e_i e_j. \quad (21)$$

Conversely, the inverse law (resistivity sense), given by

$$\boldsymbol{e} = \frac{e_c}{j_c} \left(\frac{\|\boldsymbol{j}\|}{j_c}\right)^{n-1} \boldsymbol{j} = \rho(\|\boldsymbol{j}\|)\boldsymbol{j}, \qquad (22)$$

gives

$$\frac{\partial e_i}{\partial j_j} = \rho(\|\boldsymbol{j}\|)\delta_{ij} + (n-1)\frac{\rho(\|\boldsymbol{j}\|)}{\|\boldsymbol{j}\|^2} \; j_i j_j. \qquad (23)$$

Using the law (18) for ferromagnetic materials yields,

$$\frac{\partial b_i}{\partial h_j} = \mu_0 \left[1 + \left(\frac{1}{\mu_{r0}-1} + \frac{\|\boldsymbol{h}\|}{m_0}\right)^{-1}\right] \delta_{ij}$$
$$- \frac{\mu_0}{m_0} \left[\frac{1}{\mu_{r0}-1} + \frac{\|\boldsymbol{h}\|}{m_0}\right]^{-2} \frac{h_i h_j}{\|\boldsymbol{h}\|}. \qquad (24)$$

Conversely, the inverse law, given by

$$\boldsymbol{h} = \frac{1}{2} \left(\frac{\|\boldsymbol{b}\|}{\mu_0} - \frac{\mu_{r0}m_0}{\mu_{r0}-1} + s(\|\boldsymbol{b}\|)\right) \frac{\boldsymbol{b}}{\|\boldsymbol{b}\|}, \qquad (25)$$

with

$$s(\|\boldsymbol{b}\|) = \sqrt{\left(\frac{\mu_{\text{r0}} m_0}{\mu_{\text{r0}} - 1} - \frac{\|\boldsymbol{b}\|}{\mu_0}\right)^2 + \frac{4 m_0}{\mu_{\text{r0}} - 1} \frac{\|\boldsymbol{b}\|}{\mu_0}}, \quad (26)$$

gives

$$\begin{aligned}
\frac{\partial h_i}{\partial b_j} = & \frac{1}{2}\left[\frac{1}{\mu_0} - \frac{\mu_{\text{r0}} m_0}{(\mu_{\text{r0}} - 1)\|\boldsymbol{b}\|} + \frac{1}{\|\boldsymbol{b}\|} s(\|\boldsymbol{b}\|)\right]\delta_{ij} \\
& + \frac{1}{2}\left[\frac{\mu_{\text{r0}} m_0}{(\mu_{\text{r0}} - 1)\|\boldsymbol{b}\|^3} - \frac{1}{\|\boldsymbol{b}\|^3} s(\|\boldsymbol{b}\|)\right. \\
& + \left. (s(\|\boldsymbol{b}\|))^{-1}\left(\frac{2 - \mu_{\text{r0}}}{\mu_{\text{r0}} - 1} m_0 + \frac{\|\boldsymbol{b}\|}{\mu_0}\right)\frac{1}{\mu_0 \|\boldsymbol{b}\|^2}\right] b_i b_j. \quad (27)
\end{aligned}$$

ACKNOWLEDGMENT

REFERENCES

[1] S. Nishijima, S. Eckroad, A. Marian, K. Choi, W. S. Kim, M. Terai, Z. Deng, J. Zheng, J. Wang, K. Umemoto, J. Du, P. Febvre, S. Keenan, O. Mukhanov, L. D. Cooley, C. P. Foley, W. V. Hassenzahl, and M. Izumi, "Superconductivity and the environment: a roadmap," *Superconductor Science and Technology*, vol. 26, p. 113001, sep 2013.

[2] J. H. Durrell, M. D. Ainslie, D. Zhou, P. Vanderbemden, T. Bradshaw, S. Speller, M. Filipenko, and D. A. Cardwell, "Bulk superconductors: a roadmap to applications," *Superconductor Science and Technology*, vol. 31, p. 103501, sep 2018.

[3] F. Sirois and F. Grilli, "Potential and limits of numerical modelling for supporting the development of HTS devices," *Superconductor Science and Technology*, vol. 28, no. 4, p. 043002, 2015.

[4] Z. Hong, A. M. Campbell, and T. A. Coombs, "Numerical solution of critical state in superconductivity by finite element software," *Superconductor Science and Technology*, vol. 19, pp. 1246–1252, oct 2006.

[5] R. Brambilla, F. Grilli, and L. Martini, "Development of an edge-element model for AC loss computation of high-temperature superconductors," *Superconductor Science and Technology*, vol. 20, pp. 16–24, nov 2006.

[6] E. Vinot, G. Meunier, and P. Tixador, "Different formulations to model superconductors," *IEEE Transactions on Magnetics*, vol. 36, pp. 1226–1229, jul 2000.

[7] N. Enomoto and N. Amemiya, "Electromagnetic field analysis of rectangular high Tc superconductor with large aspect ratio," *Physica C: Superconductivity*, vol. 412-414, pp. 1050–1055, oct 2004.

[8] F. Grilli, S. Stavrev, Y. LeFloch, M. Costa-Bouzo, E. Vinot, I. Klutsch, G. Meunier, P. Tixador, and B. Dutoit, "Finite-element method modeling of superconductors: From 2-D to 3-D," *IEEE Transactions on Applied Superconductivity*, vol. 15, pp. 17–25, mar 2005.

[9] A. Stenvall and T. Tarhasaari, "Programming finite element method based hysteresis loss computation software using non-linear superconductor resistivity and T-φ formulation," *Superconductor Science and Technology*, vol. 23, p. 075010, jun 2010.

[10] S. Stavrev, F. Grilli, B. Dutoit, N. Nibbio, E. Vinot, I. Klutsch, G. Meunier, P. Tixador, Y. Yang, and E. Martinez, "Comparison of numerical methods for modeling of superconductors," *IEEE Transactions on Magnetics*, vol. 38, pp. 849–852, mar 2002.

[11] G. P. Lousberg, M. Ausloos, C. Geuzaine, P. Dular, P. Vanderbemden, and B. Vanderheyden, "Numerical simulation of the magnetization of high-temperature superconductors: a 3D finite element method using a single time-step iteration," *Superconductor Science and Technology*, vol. 22, p. 055005, mar 2009.

[12] A. Stenvall and T. Tarhasaari, "An eddy current vector potential formulation for estimating hysteresis losses of superconductors with FEM," *Superconductor Science and Technology*, vol. 23, p. 125013, nov 2010.

[13] A. Morandi, "2D electromagnetic modelling of superconductors," *Superconductor Science and Technology*, vol. 25, p. 104003, sep 2012.

[14] V. Lahtinen, M. Lyly, A. Stenvall, and T. Tarhasaari, "Comparison of three eddy current formulations for superconductor hysteresis loss modelling," *Superconductor Science and Technology*, vol. 25, p. 115001, sep 2012.

[15] F. Grilli, E. Pardo, A. Stenvall, D. N. Nguyen, W. Yuan, and F. Gomory, "Computation of losses in HTS under the action of varying magnetic fields and currents," *IEEE Transactions on Applied Superconductivity*, vol. 24, pp. 78–110, feb 2014.

[16] "HTS modelling." http://www.htsmodelling.com. Accessed: 2019-02-01.

[17] J. D. Jackson, *Classical electrodynamics*. AAPT, 1999.

[18] G. Lousberg, *On the magnetic properties of bulk high-temperature superconductors containing an artificial array of holes*. PhD thesis, University of Liège, 2010.

[19] A. Bossavit, "Magnetostatic problems in multiply connected regions: some properties of the curl operator," *IEE Proceedings A-Physical Science, Measurement and Instrumentation, Management and Education-Reviews*, vol. 135, no. 3, pp. 179–187, 1988.

[20] A. Bossavit, "Whitney forms: A class of finite elements for three-dimensional computations in electromagnetism," *IEE Proceedings A-Physical Science, Measurement and Instrumentation, Management and Education-Reviews*, vol. 135, no. 8, pp. 493–500, 1988.

[21] P. Dular, C. Geuzaine, and W. Legros, "A natural method for coupling magnetodynamic h-formulations and circuit equations," *IEEE transactions on magnetics*, vol. 35, no. 3, pp. 1626–1629, 1999.

[22] P. Dular, W. Legros, and A. Nicolet, "Coupling of local and global quantities in various finite element formulations and its application to electrostatics, magnetostatics and magnetodynamics," *IEEE Transactions on Magnetics*, vol. 34, no. 5, pp. 3078–3081, 1998.

[23] P. Dular, F. Henrotte, and W. Legros, "A general and natural method to define circuit relations associated with magnetic vector potential formulations," *IEEE Transactions on Magnetics*, vol. 35, pp. 1630–1633, may 1999.

[24] E. Creusé, P. Dular, and S. Nicaise, "About the gauge conditions arising in finite element magnetostatic problems," *Computers & Mathematics with Applications*, 2018.

[25] P. Dular, "The benefits of nodal and edge elements coupling for discretizing global constraints in dual magnetodynamic formulations," *Journal of computational and applied mathematics*, vol. 168, no. 1-2, pp. 165–178, 2004.

[26] P. Lombard and G. Meunier, "A general method for electric and magnetic coupled problem in 2d and magnetodynamic domain," *IEEE Transactions on Magnetics*, vol. 28, pp. 1291–1294, mar 1992.

[27] C. Geuzaine, "Nonlinear solvers." https://gitlab.onelab.info/getdp/getdp/wikis/Nonlinear-solvers. Accessed: 2019-02-01.

[28] P. Dular, C. Geuzaine, F. Henrotte, and W. Legros, "A general environment for the treatment of discrete problems and its application to the finite element method," *IEEE Transactions on Magnetics*, vol. 34, no. 5, pp. 3395–3398, 1998.

[29] P. Dular and C. Geuzaine, "GetDP reference manual: the documentation for GetDP, a general environment for the treatment of discrete problems." http://getdp.info.

[30] C. Geuzaine and J.-F. Remacle, "Gmsh: A 3-d finite element mesh generator with built-in pre-and post-processing facilities," *International journal for numerical methods in engineering*, vol. 79, no. 11, pp. 1309–1331, 2009.

[31] D. Shantsev, Y. Galperin, and T. Johansen, "Scaling and exact solutions for the flux creep problem in a slab superconductor," *Physical Review B*, vol. 65, no. 18, p. 184512, 2002.

[32] C. Bean, "Magnetization of hard superconductors," *Physical review letters*, vol. 8, no. 6, p. 250, 1962.

[33] C. Geuzaine, A. Kameni, and A. Stenvall, "Superconductors." https://gitlab.onelab.info/doc/models/wikis/Superconductors. Accessed: 2019-02-01.

[34] E. Pardo and M. Kapolka, "3D magnetization currents, magnetization loop, and saturation field in superconducting rectangular prisms," *Superconductor Science and Technology*, vol. 30, no. 6, p. 064007, 2017.

[35] G. Meunier, *The finite element method for electromagnetic modeling*, vol. 33. John Wiley & Sons, 2010.

[36] O. Biro, "Edge element formulations of eddy current problems," *Computer Methods in Applied Mechanics and Engineering*, vol. 169, no. 3, pp. 391–405, 1999.

[37] R. Brambilla, F. Grilli, L. Martini, M. Bocchi, and G. Angeli, "A finite-element method framework for modeling rotating machines with superconducting windings," *IEEE Transactions on Applied Superconductivity*, vol. 28, pp. 1–11, Aug. 2018.

[38] K. Jacques, *Energy-Based Magnetic Hysteresis Models-Theoretical Development and Finite Element Formulations*. PhD thesis, University of Liège, 2018.